Single Pd atoms on TiO$_2$ dominate photocatalytic NO$_x$ removal

Kakeru Fujiwara[1], Sotiris E. Pratsinis[*]

Particle Technology Laboratory, Institute of Process Engineering, ETH Zurich, Sonneggstrasse 3, CH-8092 Zurich, Switzerland

ARTICLE INFO

ABSTRACT

Reducing the particle size of platinum-group metals (PGM) down to single atom can maximize catalyst performance while minimizing their use. Here Pd/TiO$_2$ particles are made by flame spray pyrolysis with closely controlled Pd-content. The fraction of Pd on the TiO$_2$ surface is determined by leaching. For 0.025–1 wt.% of nominal Pd-content, 40–70% of it is on the TiO$_2$ surface dramatically enhancing its solar-light photocatalytic NO$_x$ removal. Most importantly, the fraction of isolated Pd atoms on TiO$_2$ is quantified by diffuse reflectance infrared Fourier transform spectroscopy (DRIFTS) using NO as probing molecule and BaSO$_4$ as internal standard. Isolated Pd atoms are identified by the linear NO adsorption peak on cationic single Pd atoms. Their fraction on flame-made Pd/TiO$_2$ linearly increases up to 0.1 wt.% of nominal Pd-content and above that, formation of Pd clusters or particles takes place. In contrast, for photodeposited Pd (0.1 and 1 wt.%) on TiO$_2$, isolated Pd atoms are not found on its surface. The NO removal efficiency linearly increases with the mass fraction of isolated Pd atoms on TiO$_2$, regardless of the presence of Pd clusters or particles. The superior performance of isolated Pd sites is attributed to their high resistance to nitrate poisoning and high selectivity for the conversion of NO to nitrate compared to that of nitrate to NO$_2$.

1. Introduction

Recently, isolated PGM sites on metal oxide supports have been proposed as the active sites for various reactions to minimize PGM use [1] at high reactivity (water-gas shift [2], hydrogenation [3], dehydrogenation of alkanes [4,5] and O$_2$ reduction [6]), durability for CO poisoning [7] and selectivity (water-gas shift [8], reverse water-gas shift [9] and preferential CO oxidation [10]). Such isolated PGM atoms often coexist with their clusters or nanoparticles prepared by precipitation [8], impregnation [9] and photodeposition [11] making difficult the determination of the active sites in PGM catalysts.

Scanning transmission electron microscopy (STEM) is widely used to visualize isolated PGM atoms and their nanoparticles revealing, for example, the size-dependency of Pd [12] and Ru [13] for CO$_2$ reduction. Even though some isolated PGM atoms could be observed by STEM, it is impossible to detect all of them limiting the STEM capacity for quantitative analysis. Diffuse reflectance infrared Fourier transform spectroscopy (DRIFTS) using probe molecules such as CO [[13],8, [9],14] and NO [15] that are sensitive only for the species on the catalyst surface could reveal isolated PGM (Rh [8,[9]], Pt [14] and Pd [[13],15]) atoms facilitating the identification of active sites. For example, isolated Rh sites form a unique CO adsorption structure resulting in a characteristic DRIFTS peak [9]. Furthermore, the peaks of CO and

NO adsorption on isolated Pt [16] and Pd [15] sites, respectively, appear at higher wavenumbers than their clusters or nanoparticles. Based on these characteristic DRIFTS peaks of PGM isolated atoms and clusters, the fraction of atom (and cluster) *sites* can be calculated from their peak intensities using extinction coefficients for IR spectra of adsorbed probe molecules [9]. Finding the proper extinction coefficients, however, might be difficult as they could vary depending on the support of metals [17].

Design of PGM co-catalysts for photocatalysis is important for environmental remediation. The PGM co-catalysts (Au [18], Pd [19] and Pt [20,21]) facilitate O$_2$ reduction to O$_2^-$ by photo-excited electron transfer from photocatalysts (e.g. TiO$_2$) [22] and subsequent catalytic O$_2$ reduction [23] on their surface. Such effects can be boosted by decreasing the co-catalyst size because of the up-shift of the Fermi level [18] as well as the increase of the co-catalyst specific surface area [19].

Recently, isolated Pd atoms and subnano-clusters deposited on TiO$_2$ particles by continuous flame spray pyrolysis (FSP) [15] exhibited 3–4 times superior solar-light NO removal than photodeposited Pd nanoparticles on FSP-made and commercial TiO$_2$. In these FSP-made TiO$_2$ with 0.05–3 wt.% of Pd, both Pd subnano-clusters and single atoms were identified by DRIFTS with NO as a probing molecule but their fractions could not be quantified [15] to determine the active sites responsible for this superior photocatalytic performance.

Here, the fraction of Pd on the TiO_2 surface is determined by leaching. The mass fraction of isolated Pd atoms on FSP-made Pd/TiO_2 at various nominal Pd-contents is quantified using $BaSO_4$ as an internal DRIFTS standard and NO as a probing molecule. More specifically, the mass fraction of isolated Pd atoms on these catalysts is correlated to their photocatalytic NO removal under artificial solar light (100 mW/ cm^2). Furthermore, the presence and state of isolated Pd atoms and subnano-clusters on TiO_2 after NO removal are investigated by STEM and DRIFTS revealing the dominant activity of Pd atoms.

2. Experimental

2.1. Catalyst preparation

Titanium dioxide particles containing 0–1 wt.% Pd were prepared in one step by FSP. The same flame conditions and precursor composition are used as in our previous work [15] for consistency. The Pd-content was controlled by varying the palladium acetylacetonate (Aldrich, purity 99%) concentration (0–1.2 mM) in a 1:1 volumetric mixture of 2-ethylhexanoic acid (Aldrich, purity > 99%): acetonitrile (Aldrich, purity > 99.5%) containing 159 mM of titanium isopropoxide (Aldrich, purity > 97%). Through the FSP capillary nozzle, 3 mL/min of this precursor solution were fed, dispersed to a fine spray by 5 L/min O_2 (Pan Gas, purity > 99%) through the adjacent burner ring and ignited/ sustained by a ring-shaped premixed methane/O_2 support flame (CH_4: 1.5 L/min, O_2: 3.2 L/min) [24]. So Pd/TiO_2 particles are produced and collected on a glass-fiber filter (Whatman GF, 24.7 cm effective diameter) located 77 cm above the FSP nozzle by a gas pump (Busch Mink MM 1202 AV). For photocatalysis tests, such particles were collected for 7.5 min resulting in 170 ± 19 mg of homogeneous particle layer on the filter. To remove any products of incomplete combustion from the catalyst surface (Fig. S1), the produced powders were annealed in air at 600 °C for 2 h before any photocatalytic test and particle characterizations.

Also, 0.1 and 1 wt.% of Pd were photodeposited [25] on FSP-made pure TiO_2 that had been annealed in air at 600 °C for 2 h. Such particles were prepared by dispersing 1 g of TiO_2 made at the above FSP conditions of Pd/TiO_2 but in the absence of Pd precursor in 0.3 L of distilled water with the corresponding amount of $Pd(NO_3)_2$ solution (Alfa Aesar, Pd cont. 8.5 wt.%) for consistency with the corresponding literature [26] and sonication (Sandelin DT106, 480 W, 35 kHz) for 10 min. Furthermore, 0.1 L of ethanol (Aldrich, purity > 99.8%) was added to this suspension, stirred magnetically at 600 rpm for 30 min in dark and, subsequently, irradiated by UV light (Konrad Benda, UV-Lamp UV-8 S) for 5 h. Afterwards, the particles were separated by centrifugation at 10^4 rpm for 10 min, washed by distilled water three times and dried at 50 °C in a vacuum chamber (10 mbar) for 12 h.

For photocatalysis tests, 10 g/L of TiO_2 with photodeposited Pd were dispersed by ultrasonication (Sonics Vibra-Cell 500 W, 100 kJ, 30/ 1 s on/off pulse) in a 1:1 ethanol:water solution. Five ml/min of that suspension were fed through the same FSP capillary nozzle and dispersed to a fine spray by 5 L/min oxygen (but without ignition of the support flame) resulting in homogeneous collection of 170 ± 10 mg particles on the glass-fiber filter 62 cm above the nozzle [15].

2.2. Catalyst characterization

The specific surface area (SSA) of catalysts was obtained by N_2 adsorption at 77 K using the Brunauer-Emmett-Teller (BET) method (Micromeritics, Tristar II PULS). The STEM images of particles were recorded with a high-angle annular dark-filed detector (Hitachi, HD 2700-Cs, 200 kV). Diffuse-reflectance spectra of the catalysts were measured by a Varian Cary 500 UV–vis spectrophotometer equipped with an integrating sphere.

The X-ray diffraction (XRD) patterns of powders, with and without 20 wt.% of NiO (Aldrich, size: −325 mesh) as an internal standard

[27], were obtained by a diffractometer (AXS D8 Advance, Bruker, Cu K_α, 40 kV, 40 mA, 0.61°/min). Using the internal standard, the crystalline and amorphous fractions of TiO_2 were calculated as described elsewhere [15]. The crystalline sizes of anatase (ISDC: 663711) and rutile (ISDC: 663710) were obtained by Rietveld analysis using a software Topas 4.2. Adsorption of NO on Pd clusters and isolated atoms on TiO_2 was investigated by DRIFTS using a Vertex 70v spectrometer (Bruker Optics). The Pd/TiO_2 or TiO_2 powders were mechanically mixed in a mortar with 10–50 wt.% of $BaSO_4$ as needed to be used as internal DRIFTS standard. A KBr powder (Aldrich, FT-IR grade purity > 99%) stored in a drying oven at 120 °C (just before its use) was employed as a background. The dried KBr was placed in an *in-situ* DRIFTS cell [28] and then, $BaSO_4$ with TiO_2 or Pd/TiO_2 powders were added and grinded to disperse well with KBr. The DRIFTS cell was heated up to 110 °C in Ar (Pangas, purity > 99.999%) for 15 min and subsequently, cooled down to 50 °C. Afterwards, 200–2000 ppm of NO in N_2 was passed over the sample and IR spectra were recorded by averaging 100 scans (100 scan/min) at 4 cm^{-1} resolution. It should be noted that in contrast to [15], the exposure time was not always the same (often longer than 20 min and up to even three hours). This is because the addition of $BaSO_4$ prolonged the time to reach a steady state DRIFT spectrum (e.g. the peak at 1840–1850 cm^{-1} was unchanged) as $BaSO_4$ is sticky and heavily agglomerated that can hinder diffusion of NO to Pd/TiO_2. Here, only the spectra reacheda steady state within 50 min were used as prolonged exposure of Pd to NO might lead to reaction with bound oxygen converting $Pd-O_x$ into PdO_xN_y and shift that peak.

In FSP-made Pd/TiO_2, Pd could be present both on the TiO_2 surface as a co-catalyst and in the bulk TiO_2 (e.g. as a dopant). The fraction of Pd on the TiO_2 surface was estimated by leaching [29]. So before such leaching, Pd/TiO_2 particles were reduced under 5% of H_2 in Ar at 150 °C for 30 min. Then, 80 mg of the reduced powder was stirred in 20 mL of a 1/3.3/1.7 volumetric mixture of H_2O_2 solution (Aldrich, 30% H_2O_2 in H_2O), HCl solution (Aldrich, 34–26% in H_2O) and DI-water at 60 °C (5% H_2O_2 + 7% HCl aqueous solution) for 2 h to leach Pd from the powder surface [29]. After that, the remaining solid particles were removed by centrifugation (Hettich ROTINA 35) at 13′000 rpm for 10 min followed by filtration through a PTFE filter (Aldrich, pore size $\leq 0.2 \mu m$) to obtain a particle-free solution. The concentrations of leached Pd and Ti in solution were measured by inductively coupled plasma-optical emission spectrometry (ICP-OES, Varian 720-ES axial).

2.3. Photocatalytic evaluation for NO removal under solar-light

The photocatalytic NO removal by all catalysts under solar light (100 mW/cm^2, Solarsim 150, Solaronix) for 5 h was carried out in a continuous-flow reactor as defined by the ISO standard (ISO 22197-1:2007) described in detail elsewhere [30]. Briefly, the 5 cm × 10 cm rectangular glass-fiber filter coated with about 16 mg of catalysts (as described above) was placed in the middle part of the reactor. An air stream of 3 L/min at 50% relative humidity containing 1 ppm of NO flowed over the catalyst while NO and NO_2 concentrations were monitored every 3 s by a NO_x detector (CLD 882 S, Eco Physics) at the reactor outlet. The NO conversion (η_{NO}), NO_2 formation (η_{NO2}) and NO_x removal (η_{NOx}) efficiencies [31] are:

$$\eta_{NO} = \frac{C_{NO_{in}}[\text{ppm}] - C_{NO_{out}}[\text{ppm}]}{C_{NO_{in}}[\text{ppm}]} \cdot 100 [\%] \qquad (1)$$

$$\eta_{NO_2} = \frac{C_{NO2_{out}}[\text{ppm}]}{C_{NO_{in}}[\text{ppm}]} \cdot 100 [\%] \qquad (2)$$

$$\eta_{NO_x} = \eta_{NO} - \eta_{NO_2} [\%] \qquad (3)$$

Note that almost all of removed NO and NO_2 are converted into nitrate ion that remains on the catalyst surface as determined by these
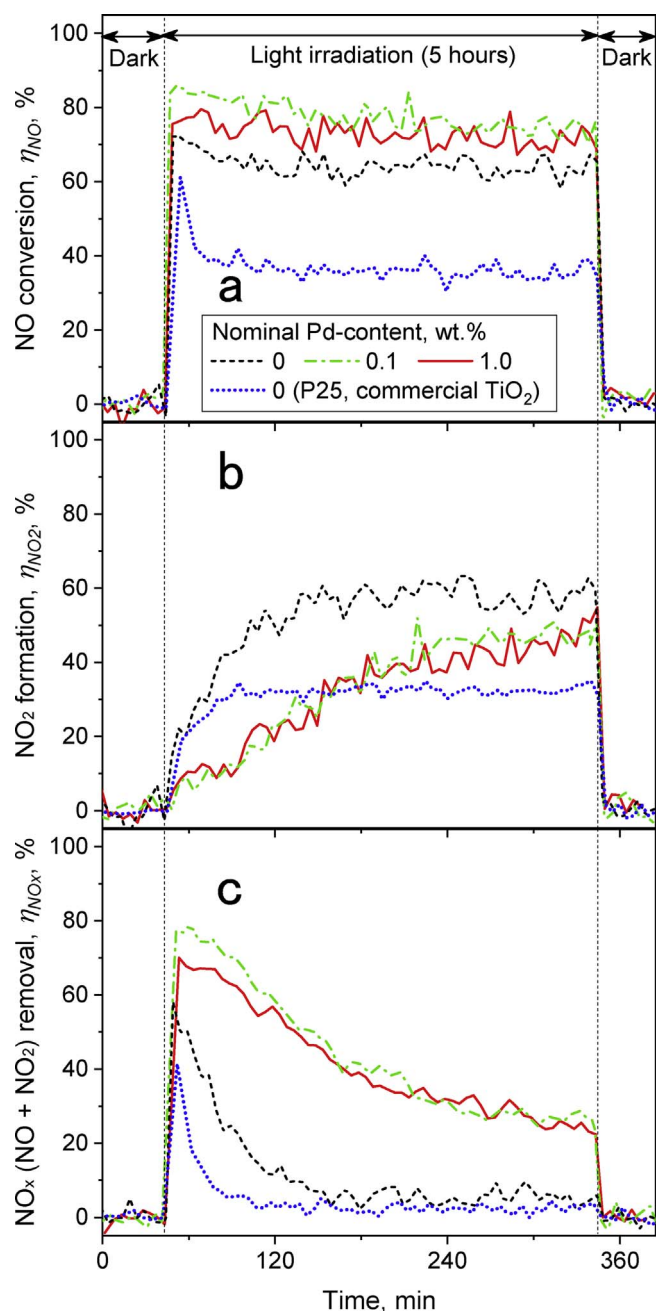
Fig. 1. Evolution of the efficiencies for (a) NO removal, η_{NO}, (b) NO$_2$ formation, η_{NO2}, and (c) NO$_x$ removal, η_{NOx}, by FSP-made TiO$_2$ with (black dotted line) 0, (red solid line) 0.1 and (green dot-broken line) 1 wt.% of Pd under artificial solar-light (100 W/cm^2). For comparison, the efficiencies by commercial TiO$_2$ (blue short-dotted line, P25, Evonik) are shown also. (For interpretation of the references to colour in this figure legend, the reader is referred to the web version of this article.)

gas measurements and electrochemically, regardless of Pd-content [15] and deposition method [30]. Also, the turnover number of total Pd content (TON_{Pd} = [NO$_x$ removed by Pd/TiO$_2$ − NO$_x$ removed by TiO$_2$]/[the amount of total Pd content]) for t = 5 h was calculated:

$$TON_{Pd} = \frac{\int_{t=0h}^{t=5h} \text{NO feedrate [mol/h]} \cdot (\eta_{NO_x} \text{ of Pd/TiO}_2 - \eta_{NO_x} \text{ of TiO}_2) \cdot dt}{Mw_{Pd} \text{[g/mol]} \cdot mass \, of \, catalysts \text{[g]} \cdot \text{Pd} - content \text{[wt.\%]}/100}$$

(4)

3. Results and discussion

3.1. Resistance to nitrate poisoning on isolated Pd atoms

Fig. 1 shows the efficiency evolution of a) NO conversion, η_{NO}, b) NO$_2$ formation, η_{NO2}, and c) NO$_x$ removal, η_{NOx}, by FSP-made TiO$_2$ with 0 (black dotted line), 0.1 (red solid line) and 1 (green dot-broken line) wt.% of Pd-content. For comparison, the efficiencies by commercial TiO$_2$ (P25, Evonik) are also shown. For the first 40 min (under dark), there is no removal of NO and formation of NO$_2$, as expected [30]. Then, under solar-light irradiation, the NO conversion (to NO$_2$ and nitrate) [32] by pure-TiO$_2$ (Fig. 1a, black line) is almost constant over the 5-h irradiation while the NO$_2$ formation increases for 80 min (Fig. 1b, black line) decreasing the NO$_x$ removal efficiency (Fig. 1c, black line). The NO conversion by FSP-made pure TiO$_2$ is almost double that by P25 that is reflected in NO$_2$ formation also. This is most likely due to the difference in SSA (P25, 51 m^2/g and FSP-made TiO$_2$, 87 m^2/g) [15]. Removed NO is accumulated on the TiO$_2$ surface as nitrate [33] accelerating NO$_2$ formation as nitrate selectively reacts with NO forming NO$_2$ photocatalytically [34]. For pure TiO$_2$, the NO$_2$ formation rate from nitrate is balanced with the conversion of NO to nitrate (~5%) within the first 80 min resulting in NO$_2$ as a main product and minor NO$_x$ removal afterwards. Hydrocarbons from incomplete combustion on the particle surface could provide additional nitrate storage mitigating nitrate coverage [33]. However, annealing (in air at 600 °C for 2 h prior to NO removal) negates this effect by removal of such hydrocarbons at 200–400 °C as determined by temperature programmed oxidation (Fig. S1).

By adding 0.1 and 1 wt% Pd on TiO$_2$ (Fig. 1, green and red lines), the NO conversion (a) is slightly higher than that by pure TiO$_2$ while NO$_2$ formation (Fig. 1b) is suppressed elucidating the beneficial effect of Pd. The actual Pd-content (0.1 or 1 wt.%), however, has less influence on the NO$_x$ removal efficiency after the first 80 min. The turnover number of NO removal in 5 h per total Pd content, TON_{Pd}, (Eq. (4)) is 65.4 and 7.6 at 0.1 and 1 wt.% of Pd, respectively. Thus, Pd catalytically enhances the NO removal efficiency but does not provide additional nitrate storage sites.

Removed NO$_x$ (NO and NO$_2$) by FSP-made Pd/TiO$_2$ is stored as nitrate on the catalyst surface as with pure [30] TiO$_2$. Notably, the initial η_{NOx} (Fig. 1c) of both FSP-made Pd/TiO$_2$ (0.1 and 1 wt.%) are only about 30% higher than that of pure TiO$_2$ indicating that Pd addition does not significantly alter the intrinsic photocatalytic activity. On the other hand, after 5 h of photocatalytic NO removal, the presence of Pd has increased drastically (4–5 times) the NO$_x$ removal efficiency, η_{NOx} over that of pure TiO$_2$ (Fig. 1c). Therefore, this superior performance of FSP-made Pd/TiO$_2$ is attributed to the persistently high selectivity of NO conversion to nitrate compared to NO$_2$ through nitrate.

Fig. 2 shows DRIFT spectra of NO adsorption on Pd/TiO$_2$ with 0 (black), 0.1 (red) and 1 (green) wt% of Pd a) before and b) after 5 h of solar-photocatalytic NO removal. In the fresh catalysts (Fig. 2a), several broad peaks associated with NO$_2$ (1470 − 1550 cm^{-1}) [35] and bidentate and bridging nitrates (1575 and 1620 cm^{-1}) [36] appear in the spectrum of pure TiO$_2$. At 1 wt.% Pd, the peaks of NO adsorption on single Pd as well as 3- and 4-fold coordinated Pd sites (1510 cm^{-1} and 1420 cm^{-1}) can be seen indicating the co-existence [15] of Pd clusters and isolated atoms on TiO$_2$. In contrast, at 0.1 wt.% Pd, only the peak of NO adsorption on single Pd atoms (1847 cm^{-1}) appears [15]. The peak position of NO adsorption on single Pd (1847 cm^{-1}) is located between metallic Pd (1750 cm^{-1}) [37] and Pd^{2+} (1860–1880 cm^{-1}) [38,39] indicating that the oxidation state of isolated Pd is Pd$^+$ or Pd^{2+}. This cationic state is due to bonding of Pd atom to several terminal O atoms on the TiO$_2$ surface forming a homogeneous Pd-O$_x$-Ti structure that is often observed in atomically-dispersed Pt and Au on ceria [2] as well as Au on titania [11] leading to Pt$^{2+,4+}$ and Au$^{+,3+}$ oxidation states.

After NO removal (Fig. 2b), all peaks corresponding to NO adsorption on TiO$_2$ (1470 − 1620 cm^{-1}) as well as 3- and 4-fold
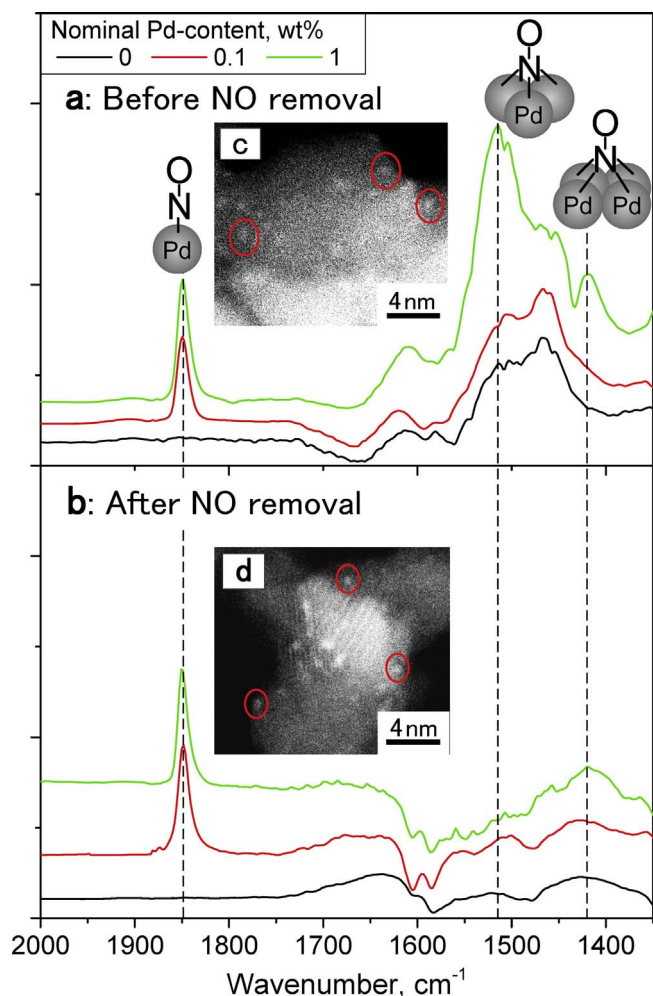
Fig. 2. DRIFT spectra of NO (1000 ppm) adsorption (after 20 min) on FSP-made Pd/TiO$_2$ with 0 (black), 0.1 (red) and 1 (green) wt.% Pd before (a) and after NO removal (b). The insets show STEM images of TiO$_2$ with 1 wt% Pd before (c) and after NO removal (d). Bright spots (red circles) and gray parts show Pd subnano-clusters and TiO$_2$, respectively. (For interpretation of the references to colour in this figure legend, the reader is referred to the web version of this article.)

Fig. 3. Fraction of leached Pd (left axis, filled symbols) from FSP-made Pd/TiO$_2$ (circles) and photodeposited Pd on TiO$_2$ (squares) in 5% H$_2$O$_2$ + 7% HCl aqueous solution at 60 °C for 2 h. All Pd on the surface is dissolved as confirmed by DRIFTS of NO (1000 ppm) adsorption on the leached samples (Fig. S3). During Pd leaching only 1–3% of TiO$_2$ is dissolved indicating no Pd dissolution form bulk TiO$_2$. The Pd fraction on the TiO$_2$ surface (right axis, open symbols) of FSP-made Pd/TiO$_2$ (circles) and photodeposited Pd on TiO$_2$ (squares) as calculated from dissolved Pd. This fraction is nearly 100% for photodeposited Pd but increases from 40% to 70% for increasing Pd-content from 0.025 to 1 wt.% for FSP-made Pd/TiO$_2$.

[7].

On FSP-made Pd/TiO$_2$, such isolated Pd atoms are present not only on the TiO$_2$ surface but also in the bulk (e.g. as a dopant) because Pd and TiO$_2$ have similar boiling points to simultaneously nucleate and grow from the vapor of Pd and Ti precursors in a flame. Fig. 3 (left axis, filled symbols) shows the fraction of leached Pd from FSP-made Pd/TiO$_2$ (circles) and photodeposited Pd on TiO$_2$ (squares). As expected, photodeposited Pd on TiO$_2$ (filled squares) is completely leached into solution. The leached Pd from FSP-made Pd/TiO$_2$ (filled circles) gradually decreases from 69 to 42% by decreasing the Pd-content from 1 to 0.025 wt.%. During leaching, only 1–3% of TiO$_2$ is dissolved regardless of Pd-content while the crystallinity of TiO$_2$ (anatase and rutile mass fractions and sizes) remains the same (Fig. S2) indicating no Pd leaching from within bulk TiO$_2$. Furthermore, all of the Pd on the TiO$_2$ surface is dissolved as confirmed by DRIFTS of NO adsorption on the leached samples (Fig. S3). Thus, the amount of leached Pd corresponds to the surface Pd concentration. Fig. 3 also shows the corresponding fraction of Pd-content on the surface (right axis) of FSP-made Pd/TiO$_2$ (open circles) and photodeposited Pd on TiO$_2$ (open squares) calculated from the dissolved Pd. The Pd surface fraction increases linearly with increasing Pd-content.

Meanwhile, up to about 1/3 of Pd (at 1 wt% of nominal Pd-content) is present in bulk TiO$_2$ that might enhance its photocatalytic activity. At 0.1 wt.% nominal Pd-content, the Pd concentration in the bulk is 0.045 wt.% (Fig. S4) that is insufficient to improve the photocatalytic activity as, according to Roy et al. [40], 0.75–1 at.% (c.a. 1–1.3 wt.%) of Pd doping to bulk TiO$_2$ is needed to overcome the photocatalytic activity of TiO$_2$ with deposited (impregnated) Pd nano-catalysts (1 at.% or 1.3 wt.%). These Pd doping concentrations (1–1.3 wt.%) are about 30 times higher than that of FSP-made Pd/TiO$_2$ (0.045 wt.%) at 0.1 wt% nominal Pd-content. Indeed such Pd doping is insufficient to improve the photocatalytic activity as the initial η_{NOx} is almost unchanged by 0.1 or 1 wt.% Pd addition (Fig. 1c). Furthermore, Pd in bulk TiO$_2$ induces visible-light absorption (Fig. S5) but its visible-light photocatalytic activity is negligible (Fig. S6). Therefore, the contribution of Pd doping (or Pd in bulk TiO$_2$) to the photocatalytic activity is minor and the Pd sites on the surface drive predominantly the high selectivity for NO to nitrate.

coordinated Pd sites (1510 cm^{-1} and 1420 cm^{-1}) practically disappear. On the other hand, NO adsorption on single Pd sites remains nearly intact regardless of Pd-content (0.1 and 1 wt.%) and its peak position and width are identical to those before NO removal (Fig. 2a). As shown in the insets in Fig. 2, Pd subnano-clusters (bright spots in red circles) before (c) and after NO removal (d) remain the same. Additionally, almost all removed NO is converted into nitrate that remains on the catalyst surface regardless of Pd-content [15]. Hence, the disappearance of NO peaks should be due to the surface coverage of TiO$_2$ and Pd clusters by nitrates, the product of NO removal [32]. This coverage gradually decreases the NO$_x$ removal efficiency of all catalysts and, in particular, pure TiO$_2$ as shown in Fig. 1c (black line) [33]. The NO$_x$ removal efficiency with 1 wt.% of Pd (Fig. 1c, green line) is slightly higher than that at 0.1 wt.% of Pd (red line) only in the first 80 min (Fig. 1). Given that the NO adsorption peak on single Pd atoms (1847 cm^{-1}) remains after NO removal, it is quite likely that deactivation of Pd clusters by nitrate coverage take place in that period. Although some single Pd sites might be poisoned during NO removal, the higher resistance of isolated Pd atoms than their clusters to nitrate poisoning contributes to the superior Pd/TiO$_2$ photocatalytic performance over that of pure TiO$_2$. Similarly high resistance for CO poisoning is reported on single Pt atoms in Pt/Cu alloys due to the cationic nature of single Pt atoms that results in weak CO adsorption on them
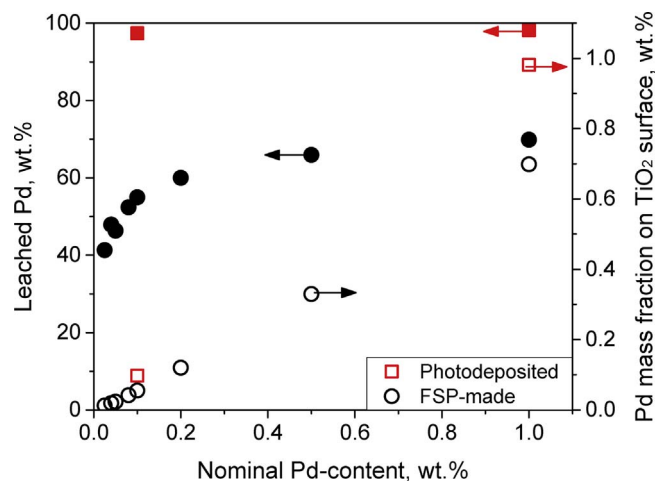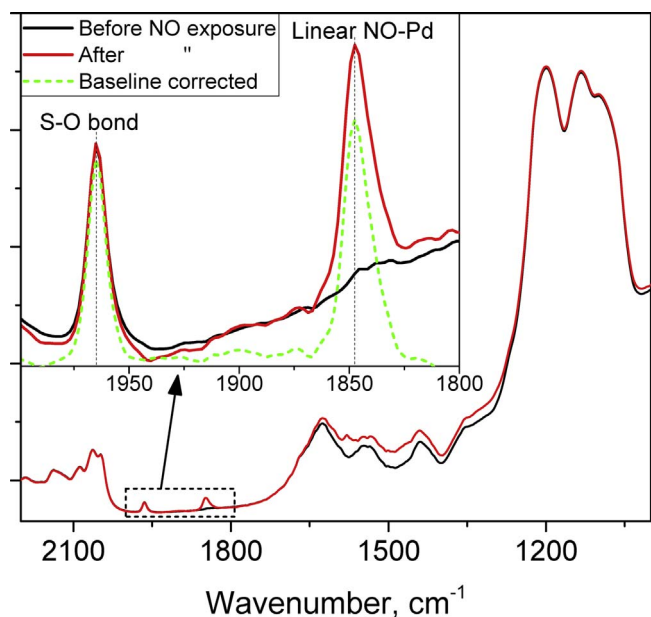
Fig. 4. DRIFT spectra of FSP-made TiO$_2$ containing 0.1 wt.% of Pd with 50 wt.% of BaSO$_4$ as internal standard before (black) and after exposure to 2000 ppm of NO for 20 min (red) to reach the equilibrium. The background was recorded with KBr. The inset shows the enlarged spectra at 1800–2000 cm^{-1} with the spectrum after NO exposure after baseline correction by the Shirley method (green broken line spectrum). The peaks at 1847 and 1967 cm^{-1} correspond to a linear NO adsorption on isolated Pd atoms [15] and a S–O bond [42] of BaSO$_4$, respectively. (For interpretation of the references to colour in this figure legend, the reader is referred to the web version of this article.)

3.2. Quantitative comparison of NO$_x$ removal by Pd atoms and clusters

Here, to quantify the mass fraction of such single Pd sites, the peak intensity of NO adsorption on single Pd sites is normalized using BaSO$_4$ as internal standard. Fig. 4 shows DRIFT spectra of FSP-made TiO$_2$ containing 0.1 wt% of Pd with 50 wt.% of BaSO$_4$ as internal standard before (black) and after (red) exposure to 2000 ppm of NO for, at least, 20 min (to reach equilibrium). Since the background was recorded with KBr, the black spectrum shows IR absorption of BaSO$_4$ and Pd/TiO$_2$ powders. After NO exposure (red spectrum), the spectrum is unaltered except at 1300–1650 cm^{-1} and 1847 cm^{-1}. These peaks are associated with NO$_2$ (1470–1550 cm^{-1}) [35] and nitrate (1575 and 1620 cm^{-1}) [36] formation on TiO$_2$ and NO adsorption on isolated Pd atoms (1847 cm^{-1}) [15]. Any peaks corresponding to NO adsorption [41] on 3- (1510 cm^{-1}) and 4-fold (1420 cm^{-1}) coordinated Pd atoms should not appear at 0.1 wt% Pd/TiO$_2$ since at this composition, the Pd exists predominantly as isolated atom sites as shown in Fig. 2a (red spectrum).

In the inset of Fig. 4, the enlarged spectra show the NO adsorption peak on isolated Pd atoms (1847 cm^{-1}) [15] and S–O bond in BaSO$_4$ (1967 cm^{-1}) [42]. Both peaks do not overlap with any other peaks and the intensity of the S–O peak remains intact after NO exposure. To compare these two peak heights, the baseline is subtracted, which does not modify the peaks as shown in the inset (green broken spectrum).

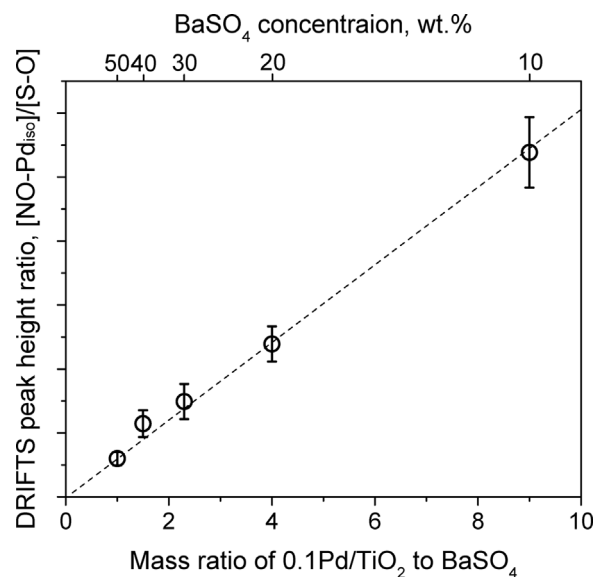Fig. 5 shows the DRIFTS peak height ratio of a linear NO adsorption on isolated Pd at 1847 cm^{-1}, [NO-Pd$_{iso}$], and a S–O bond [42] of BaSO$_4$ at 1967 cm^{-1}, [S–O], as a function of the mass ratio of 0.1 wt.% Pd/TiO$_2$ to BaSO$_4$ powder. Both heights were obtained after baseline subtraction (the blue spectrum in Fig. 4). Their ratio increases linearly with the mass ratio of Pd/TiO$_2$ to BaSO$_4$ while the intercept of the regression line (broken line) calculated by least-squares is nearly zero (= 0.0016). This means that the peak height of NO adsorption normalized by that of the S–O bond is *linearly* proportional to the population of isolated Pd sites. The error bar only at [NO-Pd$_{iso}$]/[S–O] = 9 is relatively large (e.g. 10 wt.% of BaSO$_4$) since the peak of the S–O

Fig. 5. DRIFTS peak height ratio of a linear NO adsorption on isolated Pd at 1847 cm^{-1}, [NO-Pd$_{iso}$], and a S–O bond [42] of BaSO$_4$ at 1967 cm^{-1}, [S–O], as a function of the mass ratio of FSP-made TiO$_2$ containing 0.1 wt% of Pd to BaSO$_4$ powder. Their peak heights were obtained after baseline subtraction (the green spectrum in Fig. 4).

bond is weak due to the low BaSO$_4$ content. Note that the obtained height does not absolutely correspond to 0.1 wt% of Pd on the TiO$_2$ surface since some Pd atoms are in the bulk TiO$_2$ lattice acting as dopant [43]. Nonetheless, using BaSO$_4$ as internal standard in DRIFTS enables to compare the population of isolated Pd atoms at different Pd-contents at constant BaSO$_4$ content.

Fig. 6 shows DRIFT spectra of NO adsorption on FSP-made TiO$_2$ with (a) 0.1 and (b) 1 wt.% of Pd mixed with 50 wt% of BaSO$_4$ powder under different NO concentrations (200–2000 ppm). At both Pd-content, the peak corresponding to NO adsorption on isolated Pd sites (1844 cm^{-1}) shifts to lower frequency (Δl 4.8 ~ 5.3 cm^{-1}) by decreasing the surrounding NO concentration from 2000 to 200 ppm. The peak shift takes place at 1000–2000 ppm while the peak positions below 1000 ppm seem *identical* to those at 200 ppm. Probing molecules (e.g. NO and CO) adsorbed on a metal nanoparticle induce dipole–dipole coupling that results in a large peak shift ($>$ 10 cm^{-1}) depending on the concentration of probing molecules on metal particle [44]. In contrast, the shift on isolated metal sites is much smaller (~3 cm^{-1}) than that on metal particles (NO [45] and CO [46]). Such small shift could indicate the presence of different sites on the TiO$_2$ that Pd occupies which could exhibit small shifts in the band position of adsorbed NO. These isolated atoms have slightly different bonding strength with NO broadening the peak as they have slightly different peak positions [47]. At low NO concentration, weakly bonded NO selectively desorb resulting in narrowing and shifting the peak. Indeed, regardless of Pd contents and NO concentrations, the full width at half maximum is 17–21 cm-1 that is much larger than that for probing molecules on single atom sites (Rh, 4–5 cm^{-1} [47] and Pt, 6–8 cm^{-1} [48,49]) with homogeneous atomic configurations.

To further investigate the peak at 1844–1847 cm^{-1}, its height normalized by that of the S–O bond peak (1967 cm^{-1}) of BaSO$_4$ (50 wt %), [NO-Pd$_{iso}$]$_N$, for 0.1 (filled circles) and 1 wt% Pd (filled triangles) on TiO$_2$ as a function of NO concentration (200–2000 ppm) is shown in Fig. 7. At both Pd-contents (0.1 and 1 wt.%), their [NO-Pd$_{iso}$]$_N$ peak intensities gradually increase with increasing NO concentration. As discussed already with Figs. 2 and 6, at 0.1 wt.% Pd on TiO$_2$, the Pd surface is present primarily as isolated Pd atoms on the TiO$_2$. Thus, the increase of [NO-Pd$_{iso}$] peak intensity with NO concentration (up to 1500 ppm) at this Pd-content is attributed to the shift of the equilibrium of NO ad-/desorption onto Pd: At higher NO concentration, more NO is
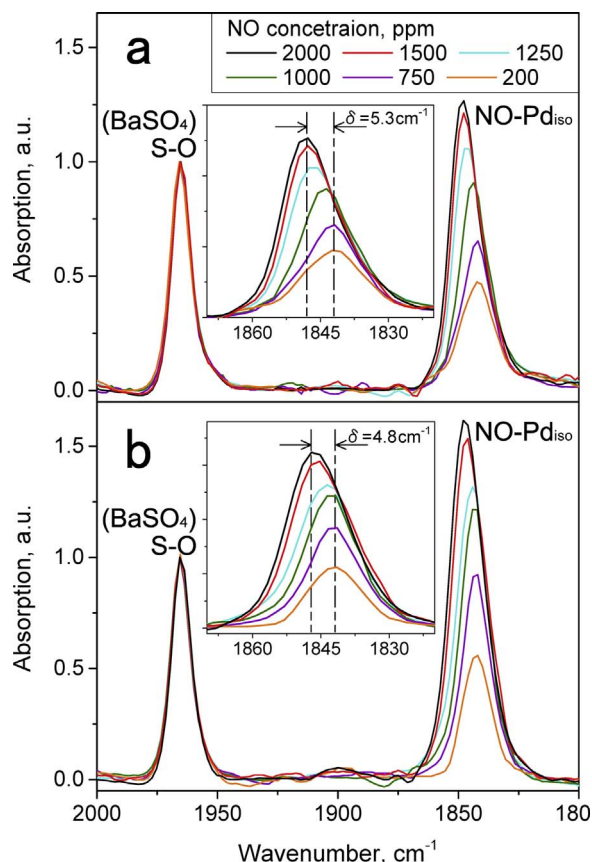
Fig. 6. DRIFT spectra of NO absorption under different NO concentration (200–2000 ppm) in FSP-made TiO_2 with (a) 0.1 and (b) 1 wt.% of nominal Pd-content with 50 wt% of $BaSO_4$ powder.
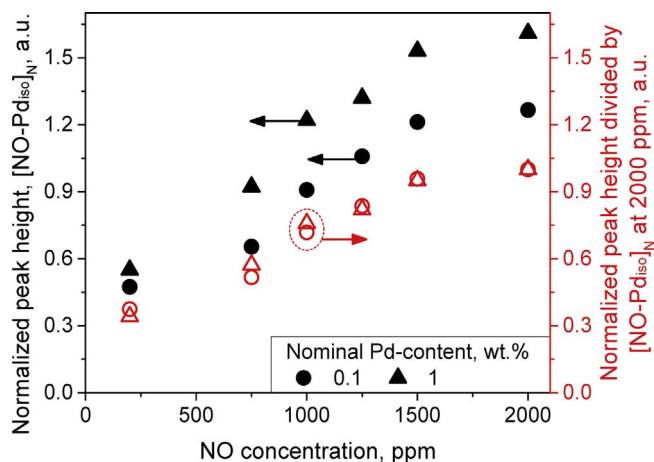

Fig. 7. DRIFTS peak height of NO adsorption on isolated Pd atoms at 0.1 (circles) and 1 (triangles) wt.% Pd on TiO_2 normalized by the S—O bond peak (1967 cm^{-1}) of $BaSO_4$ (50 wt%), $[NO\text{-}Pd_{iso}]_N$, (filled symbols) and normalized peak heights, $[NO\text{-}Pd_{iso}]_N$, divided by their heights at 2000 ppm of NO concentration (open symbols) as a function of the concentration (200–2000 ppm) of NO as probing molecule.

adsorbed on Pd increasing the peak height that levels off above 1500 ppm NO.

At 1 wt.% Pd on TiO_2, the $[NO\text{-}Pd_{iso}]_N$ peak is higher than that of 0.1 wt.% Pd on TiO_2 (Fig. 6). That increase, however, is not linear (Fig. 7). For example, a 10-fold increase in Pd concentration gives only a 25% increase in peak height, from 1.26 (Fig. 6a) to 1.63 (Fig. 6b) at 2000 ppm, indicating that only a fraction of Pd is in the form of single atoms at 1 wt.% Pd. This is expected because Pd exists both as isolated

Pd atoms and subnano-clusters that are distinguished by the peaks of the linear NO adsorption on single and multiple Pd atoms, respectively [15]. The Pd subnano-clusters result in NO adsorption on 3- and 4-fold coordinated Pd sites. Such NO adsorption structures on Pd subnano-clusters, however, could be transformed to a linear NO adsorption on single Pd atoms depending on NO concentration [50]. Because of this adsorption structure transformation, the population of NO adsorbed on single Pd atoms could change with NO concentration in the presence of Pd clusters [50].

To investigate this, the normalized peak heights, $[NO\text{-}Pd_{iso}]_N$, at 0.1 and 1 wt.% Pd are divided by their height at 2000 ppm of NO as shown in Fig. 7 (open symbols). The divided heights at both Pd-contents (0.1 and 1 wt.%) practically overlap indicating that the increase of that peak height at 1 wt.% of Pd is due to the shift of equilibrium of NO ad-/desorption as that with 0.1 wt.% of Pd and not to any transformation of the adsorption structure. Therefore, the peak at 1847 cm^{-1} is characteristic of NO adsorption on isolated Pd atoms on TiO_2. In addition, above 1500 ppm of NO, the normalized peak height reaches a plateau because of NO adsorption on all isolated Pd atoms on TiO_2. Hereafter the normalized peak height obtained with 50 wt% of $BaSO_4$ and at 2000 ppm of NO is used to quantitatively evaluate the population of isolated Pd atoms.

Fig. 8 shows the normalized peak height of NO adsorption on isolated Pd atoms, $[NO\text{-}Pd_{iso}]_N$, of FSP-made (circles) and photodeposited (squares) Pd on TiO_2 as a function of the actual Pd-content (0–1 wt.%) on the TiO_2 surface while the nominal Pd-content is written next to each symbol. For photodeposited Pd (squares), there are no isolated Pd sites so there is no detectable peak of the linear NO adsorption, regardless of Pd-content (0.1 and 1 wt.%). In contrast, the peak height of FSP-made Pd/TiO_2 linearly increases up to 0.055 wt.% actual Pd-content on the TiO_2 surface (corresponding to 0.1 wt.% nominal Pd-content). This indicates the proportional increase of isolated Pd atoms on the surface *without* Pd cluster formation up to this Pd-content. Above that (e.g. 0.2 wt.% nominal Pd-content), it gradually reaches a plateau due to formation of Pd clusters or particles [15]. Using the linear relation below 0.1 wt.% of nominal Pd-content ($[NO\text{-}Pd_{iso}]_N = 24.5\cdot$[Pd mass fraction on TiO_2 surface], $R^2 = 0.96$, in Fig. S7), the fraction of isolated Pd atoms on the surface is calculated.
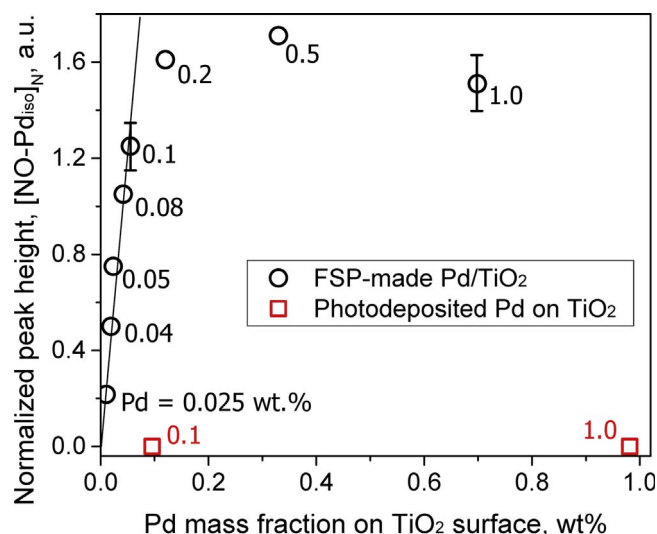
Fig. 9 shows the relation between the 5-h average solar-

Fig. 8. DRIFTS peak height of NO adsorption on isolated Pd atoms normalized by the S—O bond peak (1967 cm^{-1}) of $BaSO_4$ (50 wt%), $[NO\text{-}Pd_{iso}]_N$, of FSP-made Pd/TiO_2 (circles) and photodeposited Pd on FSP-made pure TiO_2 (squares) as a function of Pd mass fraction on the TiO_2 surface. Next to each symbol, the nominal Pd-content (0–1 wt.%) of the catalysts is written. The line indicates that the peak height corresponding to the population of isolated Pd sites on FSP-made Pd/TiO_2 increases linearly up to 0.1 wt.% of nominal Pd-content.
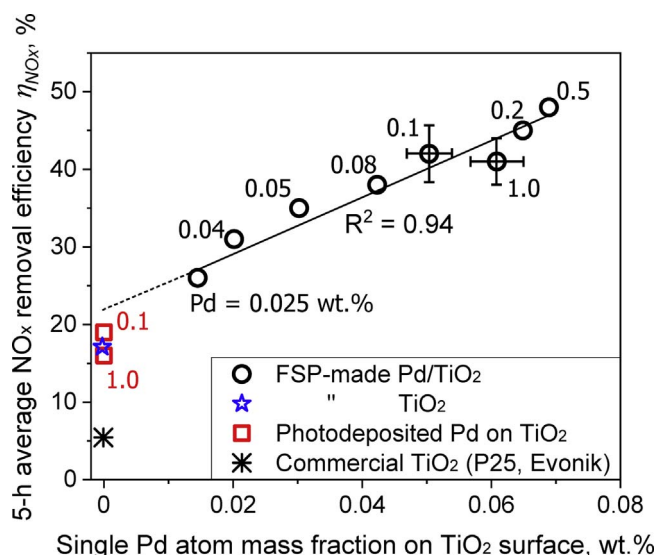
Fig. 9. Five-hour average solar-light photocatalytic NO_x removal efficiency, η_{NOx}, as a function of the isolated (single) Pd atom mass fraction on the surface (from Figs. 8 and S7) of FSP-made Pd/TiO_2 (circles) and FSP-made TiO_2 with (squares) and without (star) photodeposited Pd. Next to each symbol, the wt.% of nominal Pd-content in the Pd/TiO_2 catalysts is written. A strong correlation (solid line) is revealed between η_{NOx} and the isolated Pd atom mass fraction on FSP-made Pd/TiO_2 ($R^2 = 0.94$). Its intercept is approximately 21.8 which is close to the NO removal efficiency by FSP-made pure TiO_2 (star, 16. 5%). Note that the NO_x removal efficiency at 0.05 and 0.1–1 wt.% of Pd was obtained from our previous report [15]. For comparison, the η_{NOx} by commercial TiO_2 (P25, Evonik) is shown also.

photocatalytic NO_x removal efficiency (η_{NOx}, Eq. (3)) and the isolated Pd atom mass fraction on the surface (from Figs. 8 and S7) in FSP-made (circles) and photodeposited (squares) Pd on TiO_2 as well as FSP-made pure TiO_2 (star). The nominal Pd wt.% is written next to each symbol. Note that the average η_{NOx} at 0.05 and 0.1–1 wt.% of nominal Pd-content was obtained from our previous report [15].

Most importantly, a linear correlation (solid line) with $R^2 = 0.94$ holds between the 5-h average η_{NOx} and the isolated Pd atom mass fraction on the surface for FSP-made Pd/TiO_2. (Note that the SSA of all catalysts, 85–116 m^2/g, (Fig. S8a) is comparable.) Its intercept is approximately 21.8 that is slightly higher than the η_{NOx} by FSP-made TiO_2 (star, 16.5%) that has a higher fraction of rutile (36 wt.%, Fig. S8b) that is unfavorable for photocatalytic NO removal [51] and slightly lower SSA (87 m^2/g, Fig. S8a). Also, photodeposited Pd nanoparticles on TiO_2 (squares) hardly improve the η_{NOx} over that of pure TiO_2 (star) regardless of its Pd-content. Note that the 5-h average η_{NOx} of FSP-made Pd/TiO_2 with 1 wt.% of nominal Pd content is slightly lower than that with 0.1 wt.% of Pd, although the mass fraction of isolated Pd atoms of the former is higher than that of the later. This could be attributed to excess coverage of Pd clusters on TiO_2 which diminish photocatalytic activity [52]. Therefore, even if both Pd clusters and isolated atoms are present, the drastic enhancement of the activity by the Pd co-catalyst deposited on TiO_2 primarily originates from isolated Pd atoms. Also, the NO_x removal performance is about 10-fold better than that of commercial TiO_2 (P25, Evonik). Similar size dependency between platinum-group metal (Pt and Au) nanoparticles and isolated atoms was also found in the water-gas shift reaction [2]. Such isolated PGM atom sites with high nitrate poisoning resistance are important for air cleaning in practical environments where various compounds including NO_x are present.

4. Conclusions

The size-dependent activity of flame-made Pd co-catalysts on TiO_2 and the role of isolated Pd sites for photocatalytic NO removal are investigated. The mass fraction of Pd on the TiO_2 surface is determined by leaching while the fraction of isolated Pd atoms there is quantified using an internal DRIFTS standard ($BaSO_4$) and NO as probing molecule. The mass fraction of isolated Pd atoms in FSP-made Pd/TiO_2 linearly increases up to 0.055 wt.% of Pd on the surface (0.1 wt.% nominal Pd-content). Above that content, it reaches a plateau as Pd clusters are formed. Regardless of Pd-content, however, the 5-h average NO removal efficiency linearly increases with the mass fraction of isolated Pd atoms, indicating the minor activity of Pd clusters or particles and Pd in bulk TiO_2 (as dopant). This is attributed to the high nitrate poisoning resistance of isolated Pd sites and their high selectivity for the conversion of NO to nitrate compared to that of nitrate to NO_2. Also, FSP-made Pd/TiO_2 contains 30–60% of nominal Pd-content (1 to 0.025 wt.%, respectively) in bulk TiO_2 (e.g. Pd as dopant) but its contribution to the NO_x removal is negligible.

Author contributions

K.F. and S.E.P. contributed equally.

Conflict of interest

The authors declare no competing financial interest.

Appendix A. Supplementary data

Supplementary data associated with this article can be found, in the online version, at https://doi.org/10.1016/j.apcatb.2017.12.042.

References

[1] J. Liu, Catalysis by supported single metal atoms, ACS Catal. 7 (2017) 34–59.

[2] Q. Fu, H. Saltsburg, M. Flytzani-Stephanopoulos, Active nonmetallic Au and Pt species on ceria-based water-gas shift catalysts, Science 301 (2003) 935–938.

[3] P. Liu, Y. Zhao, R. Qin, S. Mo, G. Chen, L. Gu, D.M. Chevrier, P. Zhang, Q. Guo, D. Zang, Photochemical route for synthesizing atomically dispersed palladium catalysts, Science 352 (2016) 797–800.

[4] N. Yi, R. Si, H. Saltsburg, M. Flytzani-Stephanopoulos, Active gold species on cerium oxide nanoshapes for methanol steam reforming and the water gas shift reactions, Energy Environ. Sci. 3 (2010) 831–837.

[5] C. Wang, G. Garbarino, L.F. Allard, F. Wilson, G. Busca, M. Flytzani-Stephanopoulos, Low-temperature dehydrogenation of ethanol on atomically dispersed gold supported on ZnZrOx, ACS Catal. 6 (2015) 210–218.

[6] S. Yang, Y.J. Tak, J. Kim, A. Soon, H. Lee, Support effects in single-atom platinum catalysts for electrochemical oxygen reduction, ACS Catal. 7 (2017) 1301–1307.

[7] J. Liu, F.R. Lucci, M. Yang, S. Lee, M.D. Marcinkowski, A.J. Therrien, C.T. Williams, E.C.H. Sykes, M. Flytzani-Stephanopoulos, Tackling CO poisoning with single-atom alloy catalysts, J. Am. Chem. Soc. 138 (2016) 6396–6399.

[8] H. Guan, J. Lin, B. Qiao, S. Miao, A.Q. Wang, X. Wang, T. Zhang, Enhanced performance of Rh1/TiO2 catalyst without methanation in water-gas shift reaction, AIChE J. (2016) 2081–2088.

[9] J.C. Matsubu, V.N. Yang, P. Christopher, Isolated metal active site concentration and stability control catalytic CO2 reduction selectivity, J. Am. Chem. Soc. 137 (2015) 3076–3084.

[10] B. Qiao, J. Liu, Y.-G. Wang, Q. Lin, X. Liu, A. Wang, J. Li, T. Zhang, J. Liu, Highly efficient catalysis of preferential oxidation of CO in H2-rich stream by gold single-atom catalysts, ACS Catal. 5 (2015) 6249–6254.

[11] M. Yang, L.F. Allard, M. Flytzani-Stephanopoulos, Atomically dispersed Au-(OH)x species bound on titania catalyze the low-temperature water-gas shift reaction, J. Am. Chem. Soc. 135 (2013) 3768–3771.

[12] J.H. Kwak, L. Kovarik, J. Szanyi, Heterogeneous catalysis on atomically dispersed supported metals: CO2 reduction on multifunctional Pd catalysts, ACS Catal. 3 (2013) 2094–2100.

[13] J.H. Kwak, L. Kovarik, J. Szanyi, CO2 reduction on supported Ru/Al2O3 catalysts: cluster size dependence of product selectivity, ACS Catal. 3 (2013) 2449–2455.

[14] V.L. Zholobenko, G.-D. Lei, B.T. Carvill, B.A. Lerner, W. Sachtler, Identification of isolated Pt atoms in H-mordenite, J. Chem. Soc. Faraday Trans. 90 (1994) 233–238.

[15] K. Fujiwara, S.E. Pratsinis, Atomically dispersed Pd on nanostructured TiO2 for NO removal by solar light, AlChE J. 63 (2017) 139–146.

[16] Y. Barshad, X. Zhou, E. Gulari, Carbon monoxide oxidation under transient conditions: a Fourier-transform infrared transmission spectroscopy study, J. Catal. 94 (1985) 128–141.

[17] M.A. Vannice, S. Wang, Determination of IR extinction coefficients for linear-and bridged-bonded carbon monoxide on supported palladium, J. Phys. Chem. 85 (1981) 2543–2546.

[18] V. Subramanian, E.E. Wolf, P.V. Kamat, Catalysis with TiO2/gold nanocomposites. Effect of metal particle size on the Fermi level equilibration, J. Am. Chem. Soc. 126 (2004) 4943–4950.

[19] C.M. Wang, A. Heller, H. Gerischer, Palladium catalysis of O2 reduction by electrons accumulated on TiO2 particles during photoassisted oxidation of organic compounds, J. Am. Chem. Soc. 114 (1992) 5230–5234.

[20] D. Hufschmidt, D. Bahnemann, J.J. Testa, C.A. Emilio, M.I. Litter, Enhancement of the photocatalytic activity of various TiO2 materials by platinisation, J. Photochem. Photobiol. A: Chem. 148 (2002) 223–231.

[21] W.Y. Teoh, L. Mädler, D. Beydoun, S.E. Pratsinis, R. Amal, Direct (one-step) synthesis of TiO2 and Pt/TiO2 nanoparticles for photocatalytic mineralisation of sucrose, Chem. Eng. Sci. 60 (2005) 5852–5861.

[22] Y. Nosaka, K. Norimatsu, H. Miyama, The function of metals in metal-compounded semiconductor photocatalysts, Chem. Phys. Lett. 106 (1984) 128–131.

[23] R. Abe, H. Takami, N. Murakami, B. Ohtani, Pristine simple oxides as visible light driven photocatalysts: highly efficient decomposition of organic compounds over platinum-loaded tungsten oxide, J. Am. Chem. Soc. 130 (2008) 7780–7781.

[24] L. Mädler, W.J. Stark, S.E. Pratsinis, Simultaneous deposition of Au nanoparticles during flame synthesis of TiO2 and SiO2, J. Mater. Res. 18 (2003) 115–120.

[25] A.J. Bard, Photoelectrochemistry and heterogeneous photo-catalysis at semiconductors, J. Photochem. 10 (1979) 59–75.

[26] H. Yuzawa, T. Mori, H. Itoh, H. Yoshida, Reaction mechanism of ammonia decomposition to nitrogen and hydrogen over metal loaded titanium oxide photocatalyst, J. Phys. Chem. C 116 (2012) 4126–4136.

[27] B. Ohtani, O.O. Prieto-Mahaney, D. Li, R. Abe, What is Degussa (Evonik) P25? Crystalline composition analysis, reconstruction from isolated pure particles and photocatalytic activity test, J. Photochem. Photobiol. A: Chem. 216 (2010) 179–182.

[28] F. Hoxha, B. Schimmoeller, Z. Cakl, A. Urakawa, T. Mallat, S.E. Pratsinis, A. Baiker, Influence of support acid-base properties on the platinum-catalyzed enantioselective hydrogenation of activated ketones, J. Catal. 271 (2010) 115–124.

[29] M. Barakat, M. Mahmoud, Y. Mahrous, Recovery and separation of palladium from spent catalyst, Appl. Catal. A—Gen. 301 (2006) 182–186.

[30] K. Fujiwara, U. Müller, S.E. Pratsinis, Pd subnano-clusters on TiO2 for solar-light removal of NO, ACS Catal. 6 (2016) 1887–1893.

[31] A. Mills, C. Hill, P.K. Robertson, Overview of the current ISO tests for photocatalytic materials, J. Photochem. Photobiol. A: Chem. 237 (2012) 7–23.

[32] J.S. Dalton, P.A. Janes, N.G. Jones, J.A. Nicholson, K.R. Hallam, G.C. Allen, Photocatalytic oxidation of NOx gases using TiO2: a surface spectroscopic approach, Environ. Pollut. 120 (2002) 415–422.

[33] T. Ibusuki, K. Takeuchi, Removal of low concentration nitrogen oxides through photoassisted heterogeneous catalysis, J. Mol. Catal. 88 (1994) 93–102.

[34] Y. Ohko, Y. Nakamura, N. Negishi, S. Matsuzawa, K. Takeuchi, Photocatalytic oxidation of nitrogen monoxide using TiO2 thin films under continuous UV light illumination, J. Photochem. Photobiol. A: Chem. 205 (2009) 28–33.

[35] K. Hadjiivanov, V. Bushev, M. Kantcheva, D. Klissurski, Infrared spectroscopy study of the species arising during nitrogen dioxide adsorption on titania (anatase), Langmuir 10 (1994) 464–471.

[36] J.M. Watson, U.S. Ozkan, Adsorption characteristics of sol-gel Gd-Pd/TiO2 catalysts in reduction of nitric oxide with CH4: DRIFTS and TPD, J. Catal. 210 (2002) 295–312.

[37] K. Almusaiteer, S.S.C. Chuang, Dynamic behavior of adsorbed NO and CO under transient conditions on Pd/Al2O3, J. Catal. 184 (1999) 189–201.

[38] K.-I. Shimizu, F. Okada, Y. Nakamura, A. Satsuma, T. Hattori, Mechanism of NO reduction by CH4 in the presence of O2 over Pd-H-mordenite, J. Catal. 195 (2000) 151–160.

[39] P. Gélin, A. Goguet, C. Descorme, C. Lécuyer, M. Primet, Catalytic properties of palladium exchanged ZSM-5 catalysts in the reduction of nitrogen monoxide by methane in the presence of oxygen: nature of the active sites, in: A.F.N. Kruse, J.M. Bastin (Eds.), Stud. Surf. Sci. Catal. Elsevier, 1998, pp. 275–284.

[40] S. Roy, M.S. Hegde, N. Ravishankar, G. Madras, Creation of redox adsorption sites by Pd2+ ion substitution in nanoTiO2 for high photocatalytic activity of CO oxidation, NO reduction, and NO decomposition, J. Phys. Chem. C 111 (2007) 8153–8160.

[41] D. Loffreda, D. Simon, P. Sautet, Structure sensitivity for NO dissociation on palladium and rhodium surfaces, J. Catal. 213 (2003) 211–225.

[42] J. Manam, S. Das, Thermally stimulated luminescence studies of undoped, Cu and Mn doped BaSO4 compounds, Indian J. Pure Appl. Phys. 47 (2009) 435.

[43] B.D. Mukri, G. Dutta, U.V. Waghmare, M. Hegde, Activation of lattice oxygen of TiO2 by Pd2+ ion: correlation of low-temperature CO and hydrocarbon oxidation with structure of Ti1–xPdxO2–x (x = 0. 01–0.03), Chem. Mater. 24 (2012) 4491–4502.

[44] M.J. Weaver, S. Zou, C. Tang, A concerted assessment of potential-dependent vibrational frequencies for nitric oxide and carbon monoxide adlayers on low-index platinum-group surfaces in electrochemical compared with ultrahigh vacuum environments: structural and electrostatic implications, J. Chem. Phys. 111 (1999) 368–381.

[45] B. Pommier, P. Gelin, Infrared and volumetric study of NO adsorption on Pd-H-ZSM-5, Phys. Chem. Chem. Phys. 3 (2001) 1138–1143.

[46] A.Y. Stakheev, E. Shpiro, O. Tkachenko, N. Jaeger, G. Schulz-Ekloff, Evidence for monatomic platinum species in H-ZSM-5 from FTIR spectroscopy of chemisorbed CO, J. Catal. 169 (1997) 382–388.

[47] A.S. Hoffman, C.-Y. Fang, B.C. Gates, Homogeneity of surface sites in supported single-site metal catalysts: assessment with band widths of metal carbonyl infrared spectra, J. Phys. Chem. Lett. 7 (2016) 3854–3860.

[48] C. Asokan, L. DeRita, P. Christopher, Using probe molecule FTIR spectroscopy to identify and characterize Pt-group metal based single atom catalysts, Chin. J. Catal. 38 (2017) 1473–1480.

[49] L. DeRita, S. Dai, K. Lopez-Zepeda, N. Pham, G.W. Graham, X. Pan, P. Christopher, Catalyst architecture for stable single atom dispersion enables site-specific spectroscopic and reactivity measurements of CO adsorbed to Pt atoms, oxidized Pt clusters, and metallic Pt clusters on TiO2, J. Am. Chem. Soc. 139 (2017) 14150–14165.

[50] E. Ozensoy, W. Goodman, Vibrational spectroscopic studies on CO adsorption, NO adsorption CO + NO reaction on Pd model catalysts, Phys. Chem. Chem. Phys. 6 (2004) 3765–3778.

[51] J.Z. Bloh, A. Folli, D.E. Macphee, Photocatalytic NOx abatement: why the selectivity matters, RSC Adv. 4 (2014) 45726–45734.

[52] X. You, F. Chen, J. Zhang, M. Anpo, A novel deposition precipitation method for preparation of Ag-loaded titanium dioxide, Catal. Lett. 102 (2005) 247–250.